Computer Assisted Mechanics and Engineering Sciences, **18**: 3–21, 2011.
Copyright © 2011 by Institute of Fundamental Technological Research, Polish Academy of Sciences

Recent developments in stabilized Galerkin and collocation meshfree methods

Jiun-Shyan Chen, Sheng-Wei Chi
Department of Civil & Environmental Engineering
University of California
Los Angeles, CA 90095, USA
e-mail: jschen@seas.ucla.edu, chishengwei@ucla.edu

Hsin-Yun Hu
Department of Mathematics
Tunghai University
Taichung 407, Taiwan R.O.C.
e-mail: huhy@ thu.edu.tw

Meshfree methods have been developed based on Galerkin type weak formulation and strong formulation with collocation. Galerkin type formulation in conjunction with the compactly supported approximation functions and polynomial reproducibility yields algebraic convergence, while strong form collocation method with nonlocal approximation such as radial basis functions offers exponential convergence. In this work, we discuss rank instability resulting from the nodal integration of Galerkin type meshfree method as well as the ill-conditioning type instability in the radial basis collocation method. We present the recent advances in resolving these difficulties in meshfree methods, and demonstrate how meshfree methods can be applied to problems difficult to be modeled by the conventional finite element methods due to their intrinsic regularity constraints.

Keywords: meshfree methods, stabilization method, collocation method, reproducing kernel, radial basis function.

1. Introduction

In the past 15 years, meshfree methods have emerged into a new class of computational methods that have been applied to engineering and scientific problems with some success. Meshfree methods all share a common feature: the approximation of unknown in the partial differential equation is constructed based on scattered points without mesh connectivity. While no mesh is needed in the construction of approximation in meshfree methods, domain integration presents some difficulties if the discrete equation is formulated based on weak formulation, such as the element-free Galerkin (EFG) method [2, 3] and the reproducing kernel particle method (RKPM) [5, 37]. Employing the conventional Gauss quadrature rules in the Galerkin meshfree method does not pass the patch tests, and high order quadrature rule is needed for sufficient accuracy. Nodal integration, on the other hand, leads to rank instability and significant loss of accuracy in the numerical solution.

Rate of convergence in the Galerkin methods is determined by the order of completeness in the approximation functions as well as the order of accuracy in domain integration. Although nodal integration is a natural choice for Galerkin meshfree method due to the absence of the structured mesh, and it is particularly attractive for modeling problems with extremely large deformation where state and field variables can be stored at the nodal points, the method suffers from the loss

of stability and accuracy. A stabilized conforming nodal integration (SCNI) [13, 14] with gradient smoothing that satisfies first order integration constraint (passing linear patch test) and suppresses zero energy modes of the direct nodal integration has been proposed. The extension of SCNI to achieve higher rate of convergence has also been introduced [18]. The recent study shows that SCNI eliminates rank instability in the direct nodal integration but exhibits low frequency modes that could be excited under certain conditions. A modified SCNI with enhanced stability has been proposed [40, 41]. The extension of nodally integrated Galerkin meshfree methods to plates, shells, and large deformation problems have also been introduced in the literatures [6, 7, 14, 17, 47–49].

Alternatively, collocation on strong forms has been proposed in meshfree method, such as the radial basis collocation methods (RBCM) [20, 26, 27, 32, 45] and the reproducing kernel collocation method (RKCM) [28, 29]. From convergence standpoint, the compactly supported reproducing kernel approximations with monomial reproducibility render an algebraic convergence in RKCM, while the nonlocal RBFs with certain regularity offer exponential convergence in RBCM. Nevertheless, the linear system of RBCM is typically more ill-conditioned compared to those based on compactly supported approximations. The work in [20] shows that one can construct a localized RBF using a partition of unity function, such as the reproducing kernel enhanced radial basis function, to yield a local approximation while maintaining the exponential convergence in RBCM. This localized RBF, combined with the subdomain collocation method, has been applied to problems with local features, such as problems with heterogeneity or cracks that are difficult to be solved by RBCM [21, 50].

This paper provides an overview of the recent advances in Galerkin and collocation meshfree methods with particular emphasis on the issues mentioned above. The manuscript is organized as follows. Section 2 presents the Galerkin type meshfree method, with RKPM taken as an example, and shows its convergence properties. Domain integration of RKPM using SCNI is introduced, and the enhancement of SCNI to suppress spurious modes is discussed. Section 3 introduces meshfree method based on strong form collocation, with specific emphasis on the radial basis collocation method (RBCM) and a localized radial basis collocation method (L-RBCM) for enhanced conditioning. The convergence and stability properties of RBCM are discussed, and methods for stability improvement are presented. Extension of RBCM and L-RBCM to heterogeneous materials and fracture mechanics by a subdomain collocation is introduced. Section 4 outlines the application of RKPM to large deformation problems under the frameworks of Lagrangian RKPM and semi-Lagrangian RKPM, and demonstrates the performance of these methods in a class of problems that cannot be effectively modeled by the conventional finite element methods. Summary of the presented works and remarks on the future directions are given in Sec. 5.

2. Stabilized galerkin meshfree method

2.1. Reproducing Kernel (RK) approximation

Consider the domain of interest $\overline{\Omega} = \Omega \cup \partial\Omega$ be discretized by a set of points $S = \{\mathbf{x}_1, \mathbf{x}_2, \cdots, \mathbf{x}_{Np} | \mathbf{x}_I \in \overline{\Omega}\}$, and let the approximation of a function u, denoted by u^h, using information at discrete points in set S, be expressed in the following form:

$$u^h(\mathbf{x}) = \sum_{I=1}^{Np} \Psi_I(\mathbf{x}) d_I, \tag{1}$$

where $\Psi_I(\mathbf{x})$ is the shape function of node I positioned at $\mathbf{x}_I$, and d_I is the coefficient to be sought. In RK approximation, the construction of shape functions is based entirely on point data. The RK shape functions are constructed as follows [5, 37]:

$$\Psi_I(\mathbf{x}) = C(\mathbf{x}; \mathbf{x} - \mathbf{x}_I)\varphi_a(\mathbf{x} - \mathbf{x}_I), \tag{2}$$

where $\varphi_a(\mathbf{x}-\mathbf{x}_I)$ is the kernel function with compact support measured by the support dimension a, and $C(\mathbf{x};\mathbf{x}-\mathbf{x}_I)$ is the correction function composed of monomial bases:

$$C(\mathbf{x};\mathbf{x}-\mathbf{x}_I)=\sum_{i+j+k=0}^{p} b_{ijk}(\mathbf{x})(x_1-x_{1I})^i(x_2-x_{2I})^j(x_3-x_{3I})^k, \qquad p\geq 0, \tag{3}$$

where p represents the degree of monomial bases, and $b_{ijk}(\mathbf{x})$ are coefficients obtained by the following reproducing conditions:

$$\sum_{I=1}^{Np}\Psi_I(\mathbf{x})x_{1I}^i x_{2I}^j x_{3I}^k = x_1^i x_2^j x_3^k, \qquad i+j+k=0,1,\ldots,p. \tag{4}$$

Obtaining $b_{ijk}(\mathbf{x})$ from (4) yields the following RK shape function:

$$\Psi_I(\mathbf{x})=\mathbf{H}^{\mathrm{T}}(\mathbf{0})\mathbf{M}^{-1}(\mathbf{x})\mathbf{H}(\mathbf{x}-\mathbf{x}_I)\varphi_a(\mathbf{x}-\mathbf{x}_I), \tag{5}$$

$$\mathbf{M}(\mathbf{x})=\sum_{I=1}^{Np}\mathbf{H}(\mathbf{x}-\mathbf{x}_I)\mathbf{H}^{\mathrm{T}}(\mathbf{x}-\mathbf{x}_I)\varphi_a(\mathbf{x}-\mathbf{x}_I), \tag{6}$$

$$\mathbf{H}^{\mathrm{T}}(\mathbf{x}-\mathbf{x}_I)=[1,x_1-x_{1I},x_2-x_{2I},\ldots,(x_3-x_{3I})^p]. \tag{7}$$

In RK approximation, the kernel function φ_a has a compact support a and it determines the continuity of the approximation, for example, the cubic B-spline function has C^2 continuity. The degree of monomial basis functions p in the correction function $C(\mathbf{x};\mathbf{x}-\mathbf{x}_I)$ controls the order of completeness in the approximation, which is related to the order of consistency when introducing RK approximation to solve partial differential equations. For the moment matrix $\mathbf{M}$ to be nonsingular, the compact support of the kernel function has to be sufficiently large to keep the reproducing conditions in (4) linearly independent [15]. A typical RK discretization using circular supports is shown in Fig. 1a, where the support of node I is shaded in grey. The corresponding shape function over the node's compact support is shown in Fig. 1b.

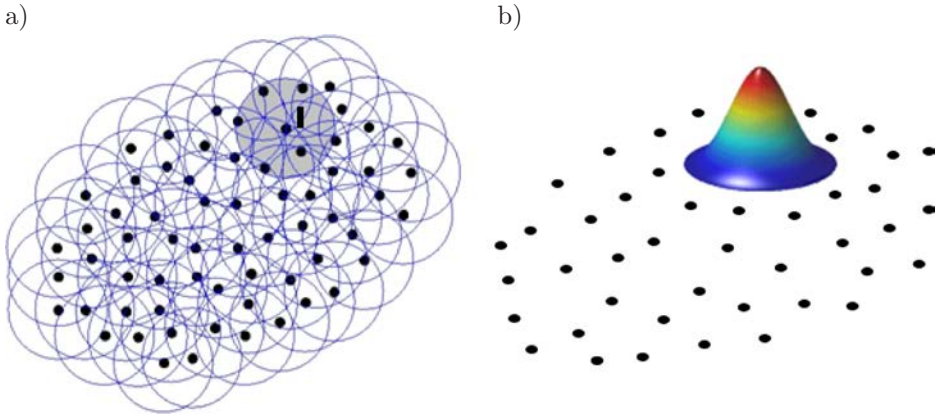

Fig. 1. a) Non-conforming RKPM discretization (support of node I shaded in grey), and b) RKPM shape function for node I.

The reproducing kernel particle method (RKPM) [37] introduces RK approximation for solving PDEs under the Galerkin framework. For demonstration, consider here a Poisson problem with Dirichlet boundary condition:

$$\nabla^2 u+Q=0 \quad \text{in } \Omega; \qquad u=g \quad \text{on } \partial\Omega. \tag{8}$$

The corresponding Galerkin approximation is to find $u^h \in H_0^1$, $\forall v^h \in H_g^1$,

$$\int_\Omega \nabla v^h \cdot \nabla u^h d\Omega = \int_\Omega v^h Q d\Omega, \tag{9}$$

where u^h and v^h are approximations of u and v, respectively. The kinematically admissible finite dimensional space H_g^1 can be obtained by coupling RK with finite element approximation [30], by transforming from generalized coordinate to nodal coordinate [5, 8, 25], or by constructing RK approximation with Kronecker delta properties [8, 15, 31]. Other methods to impose Dirichlet boundary conditions include the Lagrange multiplier method [2], the penalty method [52], and Nitsche's method [39].

The convergence of RKPM with RK approximation of degree p has been shown [15, 53] to be:

$$\left\| u - u^h \right\|_{\ell,\Omega} \leq C a^{p+1-\ell} \left| u \right|_{p+1,\Omega}, \qquad \ell \geq 0, \tag{10}$$

where a is the maximal support dimension of RK shape functions and C is independent of a and p. This algebraic convergence behaviour is very similar to that of the finite element approximation considering the proportionality of the support dimension a and the nodal distance h.

2.2. Domain integration in Galerkin meshfree method

Domain integration of weak form poses considerable complexity in Galerkin meshfree method. Employment of Gauss quadrature rules yields integration errors when background grids do not coincide with the shape function supports [23]. Direct nodal integration, on the other hand, results in rank deficiency and loss of accuracy. The above mentioned two methods do not pass linear patch test for non-uniform point distribution. A stabilized conforming nodal integration (SCNI) [13] has been introduced to ensure linear patch test and to remedy rank deficiency of direct nodal integration.

In SCNI, the gradient evaluated at the nodal point $\mathbf{x}_L$ is calculated as

$$\overline{\nabla} u^h(\mathbf{x}_L) = \frac{1}{w_L} \int_{\Omega_L} \nabla u^h d\Omega = \frac{1}{w_L} \int_{\partial\Omega_L} u^h \mathbf{n} d\Gamma, \qquad w_L = \int_{\Omega_L} d\Omega. \tag{11}$$

Here Ω_L is the nodal representative domain which can be obtained from triangulation or Voronoi cell of a set of discrete points, and $\mathbf{n}$ is the surface normal of $\partial\Omega_L$ as shown in Fig. 2.

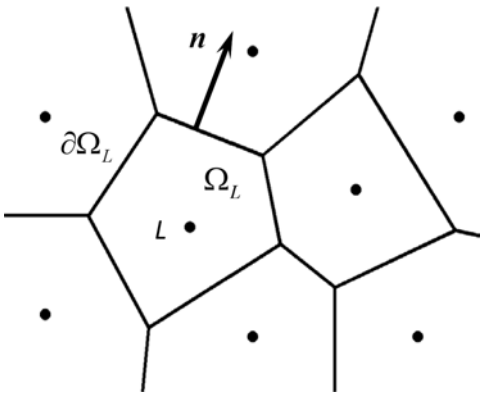

Fig. 2. Nodal representative domain.

Substituting RK approximation into (11), we have

$$\overline{\nabla} u^h(\mathbf{x}_L) = \sum_{I=1}^{N} \overline{\mathbf{B}}_I(\mathbf{x}_L) \mathbf{d}_I, \tag{12}$$

where

$$\overline{\mathbf{B}}_I(\mathbf{x}_L) = \frac{1}{w_L} \int_{\partial\Omega_L} \mathbf{n}\Psi_I d\Gamma. \tag{13}$$

Introducing the smoothed gradient of (11) into (9) and integrating the weak form by nodal integration yields the following discrete equation:

$$\sum_{L=1}^{Np} \overline{\nabla} v^h(\mathbf{x}_L) \cdot \overline{\nabla} u^h(\mathbf{x}_L) w_L = \sum_{L=1}^{Np} v^h(\mathbf{x}_L) Q(\mathbf{x}_L) w_L. \tag{14}$$

For problems with Neumann boundaries, a boundary integral on the Neumann boundary consistent with the boundary integral in (13) is employed for passing patch test; see [13] for details. A boundary value problem in Fig. 3 is solved by RKPM with first order RK approximation and with domain integrated by direct nodal integration, five-point Gauss quadrature rule, and SCNI. A much enhanced stability and convergence in SCNI compared to the direct nodal integration is observed. In fact, SCNI results are slightly better than that obtained by fifth-order Gauss quadrature.

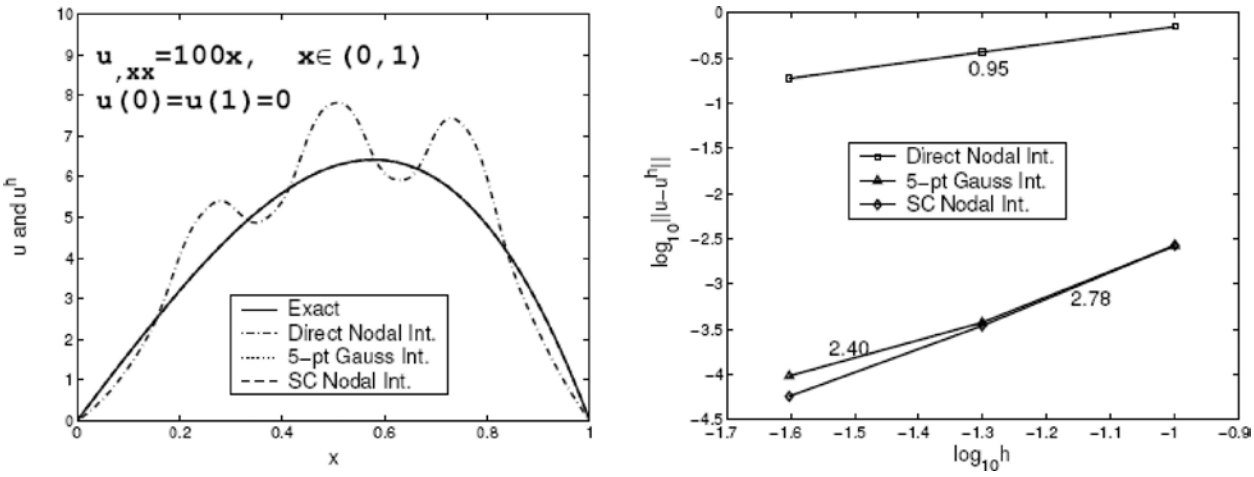

Fig. 3. Comparison of RKPM solution using various integration methods.

It has been shown that SCNI for Galerkin weak form passes linear patch test, and it eliminates zero energy modes resulting from the direct nodal integration of Galerkin weak form [13, 14]. To achieve higher order accuracy, a correction to SCNI has been proposed [18], where the left hand side of (9) is re-written as:

$$\int_\Omega \nabla v^h(\mathbf{x}) \cdot \nabla u^h(\mathbf{x}) d\Omega = \sum_{L=1}^{N} \overline{\nabla} v^h(\mathbf{x}_L) \cdot \overline{\nabla} u^h(\mathbf{x}_L) w_L + \underbrace{\sum_{L=1}^{N} \int_{\Omega_L} \Big(\nabla v^h(\mathbf{x}) - \overline{\nabla} v^h(\mathbf{x}_L)\Big) \cdot \Big(\nabla u^h(\mathbf{x}) - \overline{\nabla} u^h(\mathbf{x}_L)\Big) d\Omega}_{\text{correction term}} . \tag{15}$$

The quadratures of the correction term and the right hand side of (9) have been discussed in [18]. This approach has also been used for suppressing nonzero energy modes in SCNI, called the modified SCNI (M-SCNI), using a variant of (15) as [41]:

$$\int_{\Omega} \nabla v^h(\mathbf{x}) \cdot \nabla u^h(\mathbf{x}) d\Omega \approx \sum_{L=1}^{N} \Bigg\{ \overline{\nabla} v^h(\mathbf{x}_L) \cdot \overline{\nabla} u^h(\mathbf{x}_L) w_L + \sum_{C \in T_L} \alpha \left(\nabla v^h(\mathbf{x}_C) - \overline{\nabla} v^h(\mathbf{x}_L) \right) \cdot \left(\nabla u^h(\mathbf{x}_C) - \overline{\nabla} u^h(\mathbf{x}_L) \right) w_C \Bigg\}, \tag{16}$$

where T_L is a set of subcells associated with the Voronoi cell of node L, w_C is the corresponding area (or volume) of each subcell as shown in Fig. 4, and α is the stabilization parameter. For elasticity, a similar approach is shown in [41]. This approach can be easily applied to large deformation problems, where the nodally smoothed deformation gradient is computed using Eqs. (11)–(13). The first nonzero eigenmodes of the stiffness in two- dimensional elasticity integrated using SCNI and M-SCNI are compared in Fig. 5.

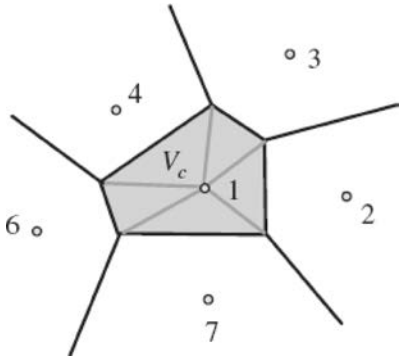

Fig. 4. Subcells of Voronoi cell.

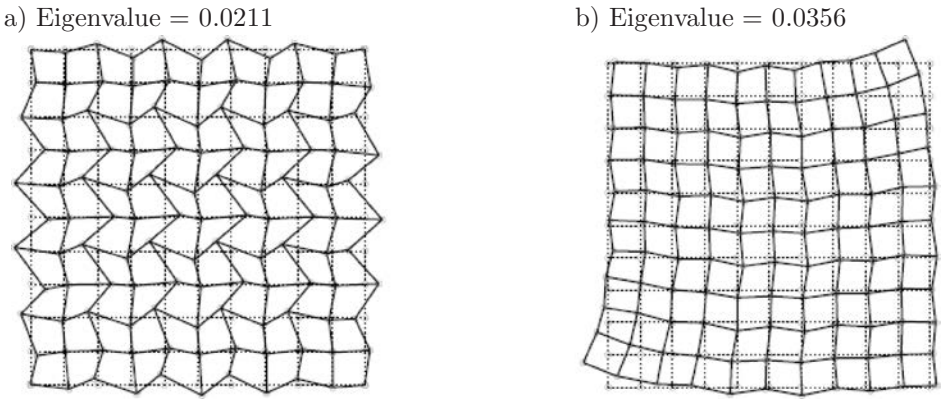

Fig. 5. First nonzero eigenmodes of RKPM in 2D elasticity generated using (a) SCNI and (b) M-SCNI.

Other stabilization methods proposed for Galerkin meshfree method include adding a residual of the equilibrium equation to the nodally integrated potential energy functional [1], the stress point method by taking derivatives away from the nodal points [42], and an approach based on iterative correction of nodal integration for patch test in conjunction with least-squares type stabilization [4].

3. Strong form collocation methods

3.1. Weighted strong form collocation method

An alternative approach to address domain integration issue in meshfree method is by collocation of strong forms. For demonstration, consider a scalar boundary value problem:

$$\begin{aligned} Lu(\mathbf{x}) &= f(\mathbf{x}) \quad \forall \mathbf{x} \in \Omega, \\ B^h u(\mathbf{x}) &= h(\mathbf{x}) \quad \forall \mathbf{x} \in \partial\Omega^h, \\ B^g u(\mathbf{x}) &= g(\mathbf{x}) \quad \forall \mathbf{x} \in \partial\Omega^g, \end{aligned} \tag{17}$$

where Ω is the problem domain, $\partial\Omega^h$ is the Neumann boundary, $\partial\Omega^g$ is the Dirichlet boundary, $\partial\Omega^h \cup \partial\Omega^g = \partial\Omega$, L is the differential operator in Ω, B^h is the differential operator on $\partial\Omega^h$, and B^g is the operator on $\partial\Omega^g$. Introducing approximation of $u^h(\mathbf{x}) = \sum_{I=1}^{N_S} g_I(\mathbf{x}) d_I$ into (17), where N_S is called the number of source points in the radial basis community (which carries the same meaning of the number of nodal points), and enforcing the residuals to be zero at the N_C collocation points $\{\boldsymbol{\xi}_J\}_{J=1}^{N_C} \in \overline{\Omega}$, we have

$$\begin{aligned} \sum_{I=1}^{N_s} Lg_I(\boldsymbol{\xi}_J) d_I &= f(\boldsymbol{\xi}_J) \quad \forall \boldsymbol{\xi}_J \in \Omega, \\ \sum_{I=1}^{N_s} B^h g_I(\boldsymbol{\xi}_J) d_I &= h(\boldsymbol{\xi}_J) \quad \forall \boldsymbol{\xi}_J \in \partial\Omega^h, \\ \sum_{I=1}^{N_s} B^g g_I(\boldsymbol{\xi}_J) d_I &= g(\boldsymbol{\xi}_J) \quad \forall \boldsymbol{\xi}_J \in \partial\Omega^g, \end{aligned} \tag{18}$$

where $g_I(\mathbf{x})$ is the approximation function. Note that Eq. (18) is an overdetermined system if $N_C > N_S$, and a least-squares method can be used for the solution. The radial basis functions (RBF) are good choice of approximation for the collocation method. The few commonly used radial basis functions are listed below:

$$\text{Multiquadrics (MQ):} \qquad g_I(\mathbf{x}) = (r_I^2 + c^2)^{n-\frac{3}{2}}, \qquad n \leq 1, \tag{19}$$

$$\text{Gaussian:} \qquad g_I(\mathbf{x}) = \exp\left(-\frac{r_I^2}{c^2}\right), \tag{20}$$

where $r_I = \|\mathbf{x} - \mathbf{x}_I\|$, and c is called the shape parameter that controls the localization of the function. There exists an exponential convergence rate of RBF given by Madych [38]:

$$\left|u(\mathbf{x}) - u^h(\mathbf{x})\right| \approx O\left(\eta_0^{c/\delta}\right) \|u\|_t, \tag{21}$$

where $0 < \eta_0 < 1$ is a real number, c is the shape parameter, and $\delta = \sup_{\mathbf{x}\in\Omega} \min_{\mathbf{x}_I \in S} \|\mathbf{x} - \mathbf{x}_I\|$, $S = [\mathbf{x}_1, \mathbf{x}_2, \cdots \mathbf{x}_{N_s} | \mathbf{x}_I \in \overline{\Omega}]$, and $\| \ \|_t$ is the induced from some properties of Fourier transformation. The accuracy and rate of convergence of MQ-RBF approximation are determined by the number of basis functions N_S (the number of source points) and the shape parameter c. The application of RBF in collocation method for PDEs is natural since RBFs are infinitely differentiable, and taking derivatives of $g_I(\mathbf{x})$ is straightforward.

The collocation method in (18) can be shown to be equivalent to the following least-squares method [27]: To seek $u^h \in V$, $V = \text{span}\{g_1, g_2, \cdots, g_{N_s}\}$, such that

$$\begin{aligned} E(u^h) &= \min_{v \in V} E(v), \\ E(v) &= \frac{1}{2} \overset{\wedge}{\int_\Omega} (Lv - f)^2 d\Omega + \frac{1}{2} \overset{\wedge}{\int_{\partial\Omega^h}} (B^h v - h)^2 d\Gamma + \frac{1}{2} \overset{\wedge}{\int_{\partial\Omega^g}} (B^g v - g)^2 d\Gamma. \end{aligned} \tag{22}$$

Here $\overset{\wedge}{\int}$ denotes the quadrature version of $\int$. For equivalence between (18) and (22), the quadrature points of numerical integration in (22) should coincide with the collocation points in (18). It has been pointed out by Hu and Chen et al. [27] that the statement in (18), and equivalently minimization of (22), yields unbalanced errors between domain and boundary collocation equations, and they proposed the following weighted least-squares method:

$$\begin{aligned} &E^*(u^h) = \min_{v\in V} E^*(v), \\ &E^*(v) = \frac{1}{2}\overset{\wedge}{\int_\Omega}(Lv-f)^2 d\Omega + \frac{\alpha_h}{2}\overset{\wedge}{\int_{\partial\Omega^h}}(B^h v - h)^2 d\Gamma + \frac{\alpha_g}{2}\overset{\wedge}{\int_{\partial\Omega^g}}(B^g v - g)^2 d\Gamma, \end{aligned} \tag{23}$$

where α^h and α^g are the weights for the Neumann boundary $\partial\Omega^h$ and Dirichlet boundary $\partial\Omega^g$, respectively. For balanced errors in the domain and on the boundaries, it was proposed [27] that the weights be selected as

$$\sqrt{\alpha^h} \approx O(1), \qquad \sqrt{\alpha^g} \approx O(\kappa N_S), \tag{24}$$

where κ is the maximum coefficient involved in the differential operator L and the boundary operator B^h. The weighted collocation formulation equivalent to the weighted least-squares formulation in (23) is

$$\begin{aligned} &\sum_{I=1}^{N_s} Lg_I(\boldsymbol{\xi}_J)d_I = f(\boldsymbol{\xi}_J) && \forall \boldsymbol{\xi}_J \in \Omega, \\ &\sqrt{\alpha^h}\sum_{I=1}^{N_s} B^h g_I(\boldsymbol{\xi}_J)d_I = \sqrt{\alpha^h}h(\boldsymbol{\xi}_J) && \forall \boldsymbol{\xi}_J \in \partial\Omega^h, \\ &\sqrt{\alpha^g}\sum_{I=1}^{N_s} B^g g_I(\boldsymbol{\xi}_J)d_I = \sqrt{\alpha^g}g(\boldsymbol{\xi}_J) && \forall \boldsymbol{\xi}_J \in \partial\Omega^g. \end{aligned} \tag{25}$$

There exists an optimal solution of the above weighted collocation method [27]:

$$\left\|u-u^h\right\|_B \le \left(C_1 N_s + C_2\sqrt{\alpha^h}N_S + C_3\sqrt{\alpha^g}\right)\|u-v\|_{1,\Omega} \le C\eta_1^{c/\delta}\|u\|_t, \tag{26}$$

where $0<\eta_0<\eta_1<1$, and

$$\|v\|_B = \left(\|Lv\|_{0,\Omega}^2 + \|v\|_{1,\Omega}^2 + \alpha^h\left\|B^h v\right\|_{0,\partial\Omega^h}^2 + \alpha^g\|B^g v\|_{0,\partial\Omega^g}^2\right)^{1/2}. \tag{27}$$

A Poisson problem $\Delta u(x,y) = (x^2+y^2)e^{xy}$ in $\Omega = (0,1)\times(0,1)$ with boundary condition $u(x,y) = e^{xy}$ on $\partial\Omega$ is solved by a direct collocation method (DCM) in (18) and the weighted direct collocation method (W-DCM) in (25) and (24), respectively, using RBFs. It is shown that the large errors on the boundaries in DCM have been corrected by W-DCM as shown in Fig. 6.

An infinite plate with a circular hole subjected to a uniform horizontal tension $\sigma_0 = 100$ N is studied next. A quarter symmetry model with domain $\overline{\Omega} \in [0,4]\times[0,4]$ is discretized by radial basis collocation method as shown in Fig. 7a and 7b, where prescribed boundary displacements on Γ_3 and Γ_4 based on analytical solution in [46] and symmetric boundary conditions on Γ_2 and Γ_5 are introduced in the model. The plane stress condition is assumed with elastic properties $E = 10^4$ Pa and $v = 0.3$. Four discretizations with 7×7, 9×9, 11×11, and 13×13 source points are used in the following convergence studies. The number of collocation points is approximately twice of

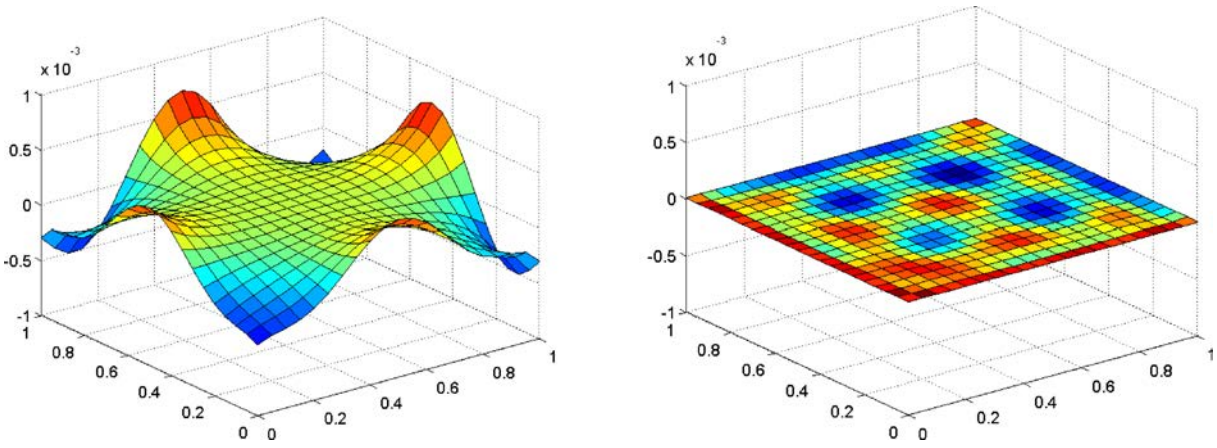

Fig. 6. The error distribution of solution obtained using DCM and W-DCM in a Poisson problem.

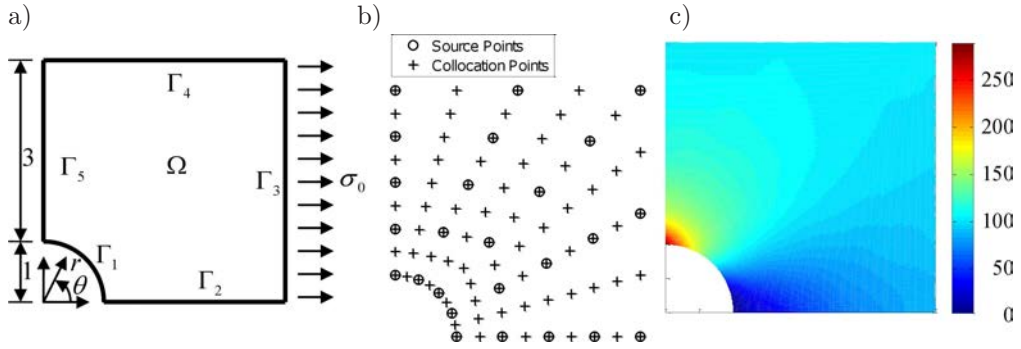

Fig. 7. a) Quarter model of an infinite plate with a circulare hole, b) discretization of the quarter model, and c) stress contour of σ_{11} obtain by W-DCM.

source points, where 13×13, 17×17, and 21×21, and 25×25 respectively, are used for the four discretizations. Based on (24), weights $\sqrt{\alpha_g} = 10^6$ and $\sqrt{\alpha_h} = 1$ are selected for W-DCM. The contour of σ_{11} obtained by W-DCM is shown in Fig. 7c, and the convergence of stress concentration in maximum relative error $\left|\sigma_{11}^h - \sigma_{11}\right| / \sigma_{11}$ is given in Table 1. The convergence of L2 norm and H1 seminorm obtained by DCM and W-DCM are compared in Fig. 8. Results show a much faster convergence in W-DCM.

Table 1. Convergence of stress concentration.

Discretization	7×7	9×9	11×11	13×13
Relative error of maximum stress	19.45%	6.27%	1.28%	0.31%

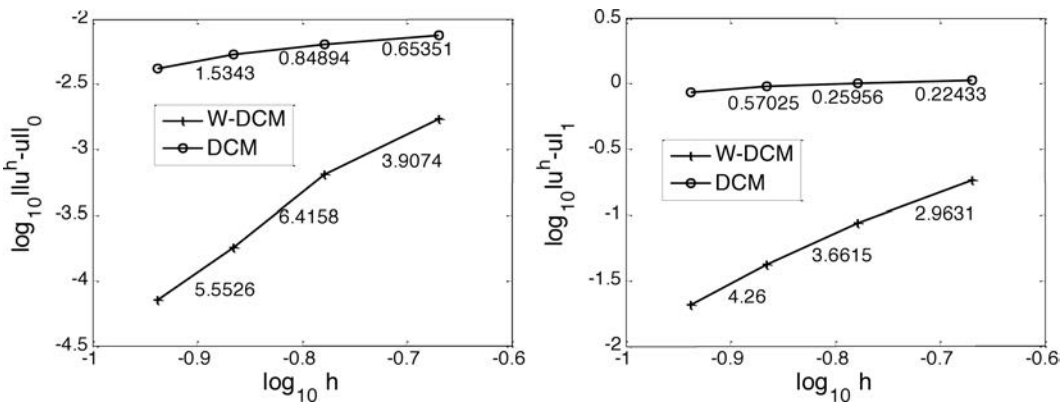

Fig. 8. Convergence of L2 error norms H1 error norms.

3.2. Localized Radial Basis Collocation Method (L-RBCM) for problems with local features

A commonly used approximation function in the strong form collocation method is the RBF, and the approach is called the radial basis collocation method (RBCM). Standard RBF offers exponential convergence, however the method suffers from the large condition numbers due to its "nonlocal" approximation. The RK functions, on the other hand, provide polynomial reproducibility in a "local" approximation, and the corresponding discrete systems are relatively well conditioned. Nonetheless, RK functions produce only algebraic convergence. An approach has been proposed to combine the advantages of RBF and RK functions to yield a local approximation that is better conditioned than that of the RBF, while at the same time offers a higher rate of convergence than that of RK [20]. This approach is shown below:

$$u^h(\mathbf{x}) = \sum_{I=1}^{N_S} \left[\Psi_{\mathrm{I}}(\mathbf{x}) \left(a_I + \sum_{J=1}^{M} g_I^J(\mathbf{x}) d_I^J \right) \right], \tag{28}$$

where $\Psi_I(\mathbf{x})$ is the RK function with compact support, and $g_I^J(\mathbf{x})$ is the RBF. Applying approximation in (28) to the weighted strong form collocation is called the localized radial basis collocation method (L-RBCM) [20].

The above approximation utilizes the compactly supported partition of unity to "patch" the global RBFs together. The error analysis shows that if the error of RK is sufficiently small, the proposed method maintains the exponential convergence of RBF, while significantly improving the conditioning of the discrete system and yielding a banded matrix [20] as discussed below.

1. Using the partition of unity properties of the RK localizing function, there exists the following error bound [20]:

   $$\|u - u_I^h\|_{0,\Omega} \leq \beta C \eta_0^{c/\delta} \|u\|_t, \tag{29}$$

   where β is the maximal number of covers for RK localizing function. Other parameters are the same as what has been defined earlier.

2. The enhanced stability in the L-RBCM can be demonstrated by a perturbation analysis of the strong form collocation equations in (25) expressed in the following linear system:

   $$\mathbf{F}\mathbf{y} = \mathbf{r}. \tag{30}$$

   The stability of the above linear system can be measured by the condition number of $\mathbf{F}$. The work in [20] obtained the following estimation of the condition number of L-RBCM:

   $$\mathrm{Cond}(\mathbf{F}) \approx O\left(a^{-3d/2}\right), \tag{31}$$

   where d is the space dimension. In two-dimensional elasticity, we have the following comparison of condition numbers using RBCM with pure RBF in (19), RKPM with pure RK in (5), and L-RBCM with localized RBF in (28) [20]:

   $$\begin{aligned} &\text{RBCM}: && \mathrm{Cond}(\mathbf{F}) \approx O(h^{-8}), \\ &\text{RKPM}: && \mathrm{Cond}(\mathbf{F}) \approx O(h^{-2}), \\ &\text{L-RBCM}: && \mathrm{Cond}(\mathbf{F}) \approx O(h^{-3}). \end{aligned} \tag{32}$$

   The L-RBCM approach offers a significant improvement on stability over RBCM. Although the discrete system of L-RBCM is slightly less well-conditioned than that of RKPM, it offers a higher convergence rate similar to that in RBCM.

The L-RBCM approach, combined with the subdomain collocation method, has been applied to problems with local features, such as problems with heterogeneity (weak discontinuity) or cracks (strong discontinuity). We describe the main ideas in the followings.

Take heterogeneous elasticity as an example as shown in Fig. 9, the following subdomain radial basis collocation method has been introduced [21]:

$$\begin{cases} \mathbf{L}^+\mathbf{u}^+ = \mathbf{f}^+ & \text{in } \Omega^+, \\ \mathbf{B}_g^+\mathbf{u}^+ = \mathbf{g}^+ & \text{on } \partial\Omega^+ \cap \partial\Omega^g, \\ \mathbf{B}_h^+\mathbf{u}^+ = \mathbf{h}^+ & \text{on } \partial\Omega^+ \cap \partial\Omega^h, \end{cases} \tag{33}$$

$$\begin{cases} \mathbf{L}^-\mathbf{u}^- = \mathbf{f}^- & \text{in } \Omega^-, \\ \mathbf{B}_g^-\mathbf{u}^- = \mathbf{g}^- & \text{on } \partial\Omega^- \cap \partial\Omega^g, \\ \mathbf{B}_h^-\mathbf{u}^- = \mathbf{h}^- & \text{on } \partial\Omega^- \cap \partial\Omega^h, \end{cases} \tag{34}$$

$$\begin{cases} \mathbf{u}^+ - \mathbf{u}^- = \mathbf{0} \\ \mathbf{B}_h^+\mathbf{u}^+ + \mathbf{B}_h^-\mathbf{u}^- = \mathbf{0} \end{cases} \quad \text{on } \Gamma. \tag{35}$$

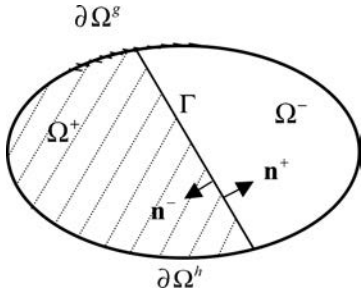

Fig. 9. Two subdomains of a problem with heterogeneity.

The solution in each subdomain is approximated by separate sets of basis functions:

$$u_i^h(\mathbf{x}) = \begin{cases} u_i^{h+}(\mathbf{x}) = g_1^+(\mathbf{x})a_{i1}^+ + \cdots + g_{N_S^+}^+(\mathbf{x})a_{iN_S^+}^+, & \mathbf{x} \in \overline{\Omega}^+, \\ u_i^{h-}(\mathbf{x}) = g_1^-(\mathbf{x})a_{i1}^- + \cdots + g_{N_S^-}^-(\mathbf{x})a_{iN_S^-}^-, & \mathbf{x} \in \overline{\Omega}^-. \end{cases} \tag{36}$$

Here, Dirichlet and Neumann types of interface conditions are introduced on the interface in (35) for optimal convergence [21]. For elasticity, (35) refers to as the displacement continuity and traction equilibrium. Localized radial basis functions have been introduced in this subdomain collocation method for enhanced accuracy [21]. An inclusion problem shown in Fig. 10 is solved by RBCM,

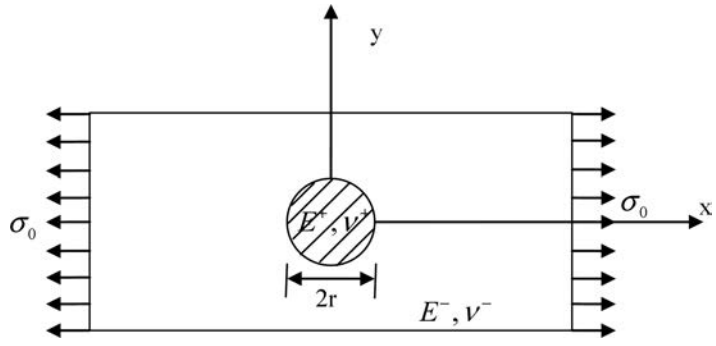

Fig. 10. Plate with circular inclusion subjected to horizontal traction.

the subdomain RBCM (SD-RBCM), and subdomain collocation method with localized radial basis functions (SD-LRBCM). Total of 330 source points and 1320 collocation points are used in a quarter model. The results in Fig. 11 show that RBCM completely missed the materials interface due to its nonlocal approximation, while both SD-RBCM and SD-LRBCM offer much enhanced accuracy.

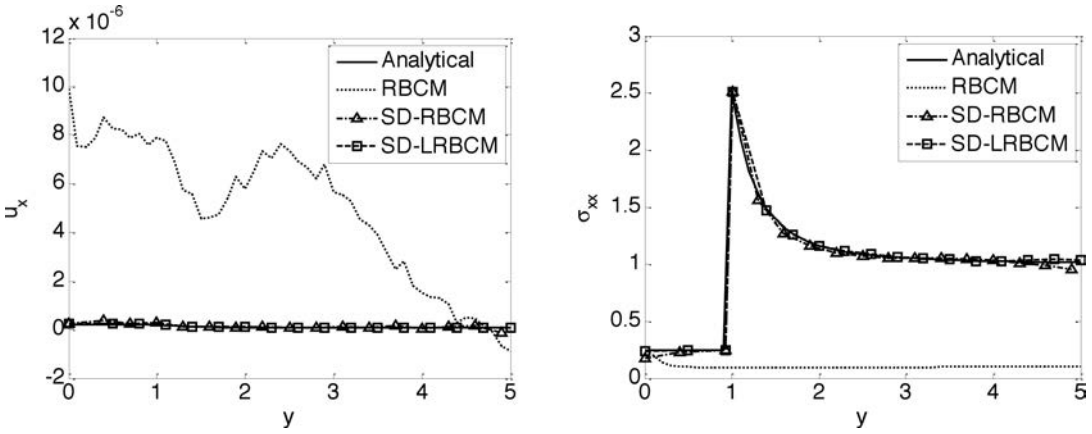

Fig. 11. Displacement and stress solutions obtained by RBCM, SD-RBCM, and SD-LRBCM.

This SD-RBCM approach has also been applied to fracture mechanics, in which the domain is sub-divided into a near-tip and far-field subdomains as shown in Fig. 12. The optimal dimension for the near-tip subdomain has been derived based on balanced errors at the triple junction [21]. Interface conditions in Eq. (35) are introduced on the interfaces of subdomains. Figure 13 demonstrates a tensile specimen with edge crack analyzed by RBCM, RBCM with visibility criteria (RBCM-VC), and the proposed SD-RBCM. The numbers of source points in the subdomains for SD-RBCM are $N_S^1 = 26$, $N_S^2 = N_S^3 = 150$, and the corresponding numbers of collocation points are $N_C^\alpha = 4N_S^\alpha$,

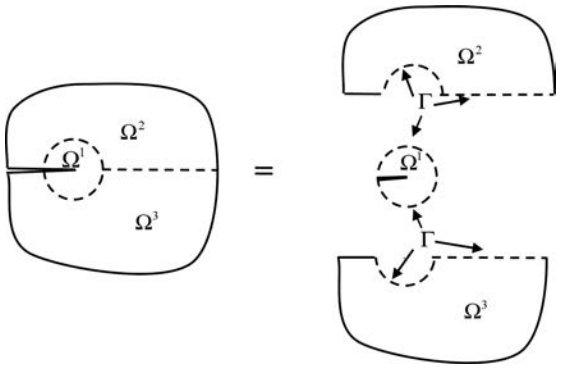

Fig. 12. Edge crack plate subjected to tension analyzed by different collocation methods.

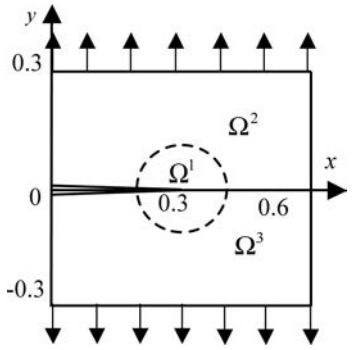

Fig. 13. Domain partitioning in crack problem.

$\alpha = 1, 2, 3$, respectively. A finite element solution with a very refined discretization of 22500 nodes is used as a reference solution. The numerical results showing a superior accuracy in SD-RBCM compared to other methods are given in Fig. 14.

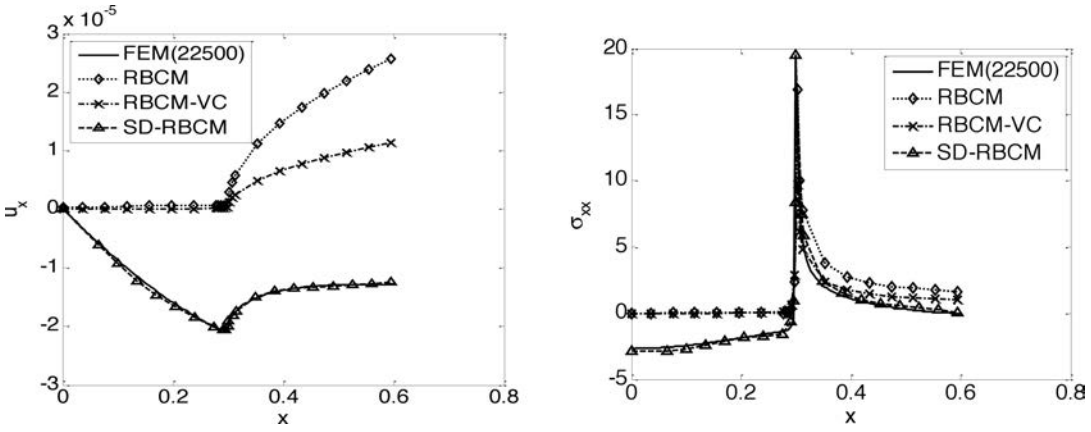

Fig. 14. Edge crack in a specimen subjected to tension.

Finally, a strong form collocation method using reproducing kernel approximation, called the reproducing kernel collocation method (RKCM), has been proposed to enhance the stability of RBCM. The error estimate provided in [28] shows that the polynomial degree of greater than one is needed in RKCM for convergence, which is different from the Galerkin type meshfree method, such as RKPM. A stability analysis of RKCM on the conditioning of the discrete system has been derived [29]. The stability analyses, validated with numerical tests, show that RKCM yields a linear system with conditioning similar to the very well-conditioned finite element discrete system.

4. Large deformation problems and other applications

The stabilized RKPM has been applied to various large deformation and fragment-impact problems. To describe the basic formulation of RKPM for large deformation problems, a material motion $\mathbf{x}_I = \boldsymbol{\phi}(\mathbf{X}_I, t)$ is considered, where $\mathbf{X}$ is the material coordinate, $\mathbf{x}$ is the spatial coordinate, t is time, and $\boldsymbol{\phi}$ is the mapping function between $\mathbf{X}$ and $\mathbf{x}$. The Lagrangian and semi-Lagrangian RKPM frameworks are outlined as follows.

1. Lagrangian RKPM formulation [5, 7, 14].
   In Lagrangian RKPM, the kernel function and basis functions are expressed in terms of material coordinate defined in the undeformed configuration, and the support of kernel function covers the same set of material points throughout deformation as shown in Fig. 15. The Lagrangian RK approximation is then introduced in the total Lagrangian formulation of conservation equations as shown in Table 2 to form the discrete equations of Lagrangian RKPM. The SCNI domain integration is performed in the undeformed configuration with the smoothing of deformation gradient at nodal point shown as follows [14]:

$$\overline{F}^h_{ij}(\mathbf{X}_L) = \frac{1}{A_L}\int\limits_{\Omega_L} F^h_{ij} d\Omega = \frac{1}{A_L}\int\limits_{\Omega_L} \frac{\partial u^h_i}{\partial X_j} d\Omega + \delta_{ij} \equiv \overline{e}_{ij}(\mathbf{X}_L) + \delta_{ij}, \qquad A_L = \int\limits_{\Omega_L} d\Omega, \tag{37}$$

$$\overline{e}_{ij}(\mathbf{X}_L) = \sum_I \overline{b}^L_{jI} d_{iI}, \qquad \overline{b}^L_{iI} = \frac{1}{A_L}\int\limits_{\Gamma_L} \Psi^X_I N_i d\Gamma, \tag{38}$$

   where Ψ^X_I is the Lagrangian RK shape function given in Table 3, and N_i is the surface normal of the nodal representative domain defined in the undeformed configuration. Lagrangian RKPM formulation works well for small to medium level deformation.

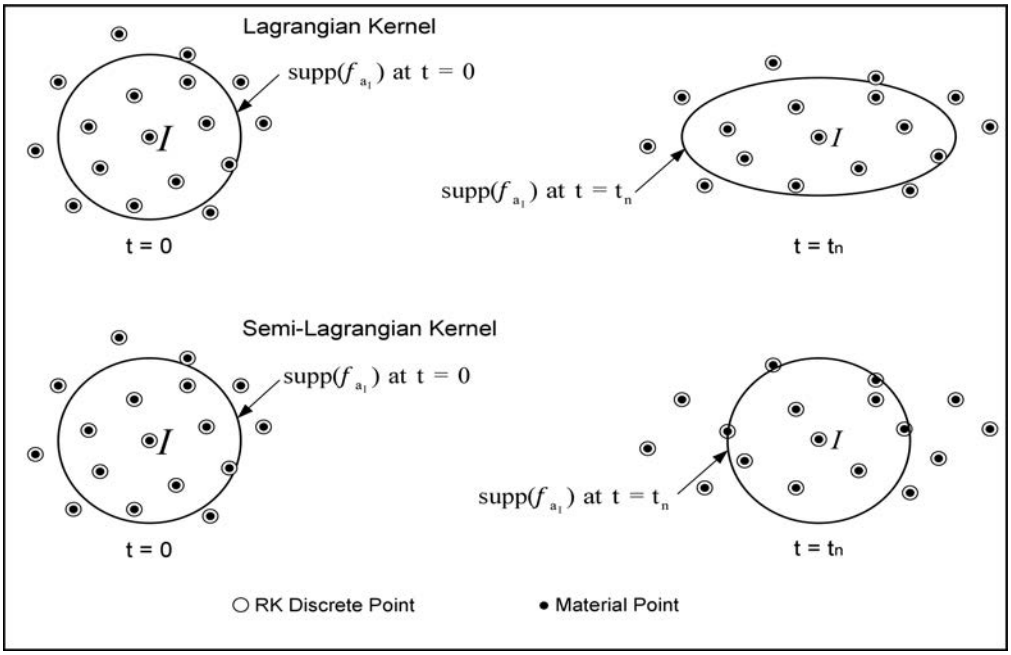

Fig. 15. Comparison of Lagrangian and semi-Lagrangian kernels.

Table 2. Total and Updated Lagrangian formulation of conservation equations.

	Total Lagrangian	Updated Lagrangian
Equation of Motion	$\int_{\Omega_X} \delta u_i \rho^0 \ddot{u}_i d\Omega + \int_{\Omega_X} \delta F_{ij} P_{ji} d\Omega = \int_{\Omega_X} \delta u_i b_i^0 d\Omega + \int_{\Gamma_X^h} \delta u_i h_i^0 d\Gamma$	$\int_{\Omega_x} \delta u_i \rho \ddot{u}_i d\Omega + \int_{\Omega_x} \delta u_{(i,j)} \tau_{ij} d\Omega = \int_{\Omega_x} \delta u_i b_i d\Omega + \int_{\Gamma_x^h} \delta u_i h_i d\Gamma$
Displacements	$u_i = x_i - X_i$: material displacement, $\ddot{u}_i = \frac{D^2 u_i}{Dt^2}$: material acceleration	
Strains/deformation	$F_{ij} = \partial x_i / \partial X_j$	$u_{(i,j)} = (\partial u_i / \partial x_j + \partial u_j / \partial x_i)/2$
Stresses	P_{ij}: first Piola-Kirchhoff stress	τ_{ij}: Cauchy stress
Other variables	ρ^0: initial density b_i^0: body force defined in the undeformed domain Ω_X h_i^0: surface traction mapped onto the undeformed traction boundary Γ_X^h	ρ: density at the current state b_i: body force defined in the deformed domain Ω_x h_i: surface traction defined on the deformed traction boundary Γ_x^h
Domains & boundaries	Ω_X: undeformed domain Γ_X^h: undeformed traction boundary	Ω_x: deformed domain Γ_x^h: deformed traction boundary

2. Semi-Lagrangian RKPM formulation [19, 22, 24].
Lagrangian RKPM breaks down in fragment-impact type problems where deformation gradient becomes non-positive definite, and semi-Lagrangian RKPM has been proposed for problems with extremely large deformation, damage, and fragmentation [19, 22, 24]. Contrary to the Lagrangian formulation, the kernel function and basis functions in semi-Lagrangian RK are expressed in terms of spatial coordinate defined in the deformed configuration as shown in

Table 3. Lagrangian and Semi-Lagrangian RK approximation.

	Lagrangian	Semi-Lagrangian
RK approximation	$u_i^h(\mathbf{X},t)=\sum_{I=1}^{NP}\Psi_I^X(\mathbf{X})d_{iI}(t)$	$u_i^h(\mathbf{x},t)=\sum_{I=1}^{NP}\Psi_I^x(\mathbf{x})d_{iI}(t)$
Approximation function	$\Psi_I^X(\mathbf{X})=\mathbf{H}^T(\mathbf{0})\mathbf{M}^{-1}(\mathbf{X})$ $\cdot\mathbf{H}(\mathbf{X}-\mathbf{X}_I)\varphi_a^X(\mathbf{X}-\mathbf{X}_I)$	$\Psi_I^x(\mathbf{x})=\mathbf{H}^T(\mathbf{0})\mathbf{M}^{-1}(\mathbf{x})$ $\cdot\mathbf{H}(\mathbf{x}-\mathbf{x}_I)\varphi_a^x(\mathbf{x}-\mathbf{x}_I)$ $\mathbf{x}_I=\boldsymbol{\phi}(\mathbf{X}_I,t)$, $\boldsymbol{\phi}$: mapping function
Kernel function	$\varphi_a^X(z),\quad z=\|\mathbf{X}-\mathbf{X}_I\|/a_I$	$\varphi_a^x(z),\quad z=\|\mathbf{x}-\mathbf{x}(\mathbf{X}_I,t)\|/a_I$
Basis functions	$\mathbf{H}^T(\mathbf{X}-\mathbf{X}_I)$ $=[1\quad X_1-X_{1I}\quad X_2-X_{2I}\ \cdots\ (X_3-X_{3I})^n]$	$\mathbf{H}^T(\mathbf{x}-\mathbf{x}_I)$ $=[1\quad x_1-x_{1I}\quad x_2-x_{2I}\ \cdots\ (x_3-x_{3I})^n]$
Moment matrix	$\mathbf{M}(\mathbf{X})$ $=\sum_{I=1}^{NP}\mathbf{H}(\mathbf{X}-\mathbf{X}_I)\mathbf{H}^T(\mathbf{X}-\mathbf{X}_I)\varphi_a^X(\mathbf{X}-\mathbf{X}_I)$	$\mathbf{M}(\mathbf{x})$ $=\sum_{I=1}^{NP}\mathbf{H}(\mathbf{x}-\mathbf{x}_I)\mathbf{H}^T(\mathbf{x}-\mathbf{x}_I)\varphi_a^x(\mathbf{x}-\mathbf{x}_I)$

Table 3. The support of kernel function could cover different set of material points throughout the deformation process as shown in Fig. 15. Let the velocity v_i be approximated by semi-Lagrangian RK shape functions:

$$v_i^h(\mathbf{x},t)=\sum_{I=1}^{NP}\Psi_I^x(\mathbf{x})v_{iI}(t), \tag{39}$$

where Ψ_I^x is the semi-Lagrangian RK shape function given in Table 3. The corresponding semi-Lagrangian approximation of acceleration is given as

$$\ddot{u}_i^h(\mathbf{x},t)=\dot{v}_i^h(\mathbf{x},t)=\sum_{I=1}^{NP}(\Psi_I^x(\mathbf{x})\dot{v}_{iI}(t)+\Psi_I^{x^*}h\mathbf{x})v_{iI}(t)), \tag{40}$$

where $\Psi_I^{x^*}(\mathbf{x})$ is the correction due to the time rate of the semi-Lagrangian kernel $\dot{\varphi}_a^x$, see [19] for details. The semi-Lagrangian RK functions in Table 3 are then introduced into the Updated Lagrangian forms of conservation equations in Table 2 to construct the discrete equations of semi-Lagrangian RKPM. The temporal stability analysis of Lagrangian and semi-Lagrangian RKPM equations of motion has been conducted in [19] for explicit time integration.

We first introduce Lagrangian RKPM to model a Taylor bar impact problem stated in Fig. 16. The problem definition can be found in [5], and the results of Lagrangian RKPM [5] and three-

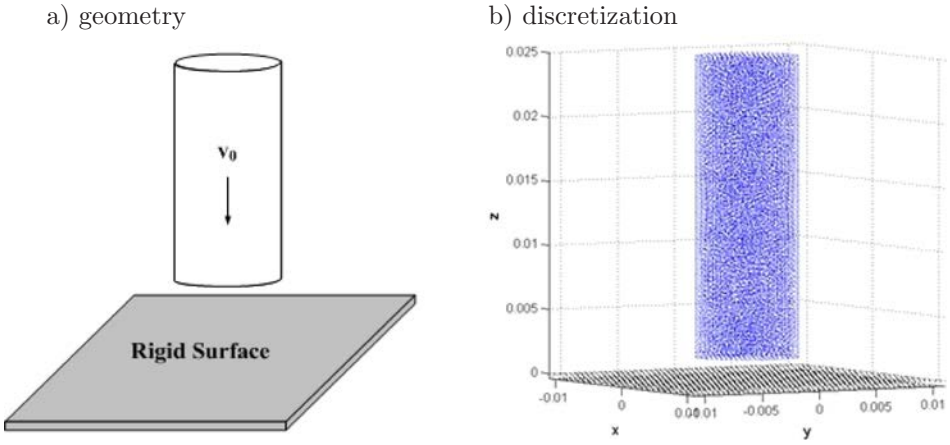

Fig. 16. Taylor bar impact problem definition.

dimensional semi-Lagrangian RKPM with 29,788 nodes are shown in Fig. 17 and Table 4. Next, we introduce the semi-Lagrangian RKPM to model the process of a bullet penetrating through a concrete plate given in [44]. In this simulation, a micro-crack informed damage model [43] has been used in conjunction with the stabilization methods discussed in Secs. 2 and 4. A semi-Lagrangian RKPM model with the projectile and panel discretized using 1,163 nodes and 190,000 nodes, respectively, is used. The numerical and experimental damage patterns of the exit face [44] are compared in Fig. 18, and good agreement is observed.

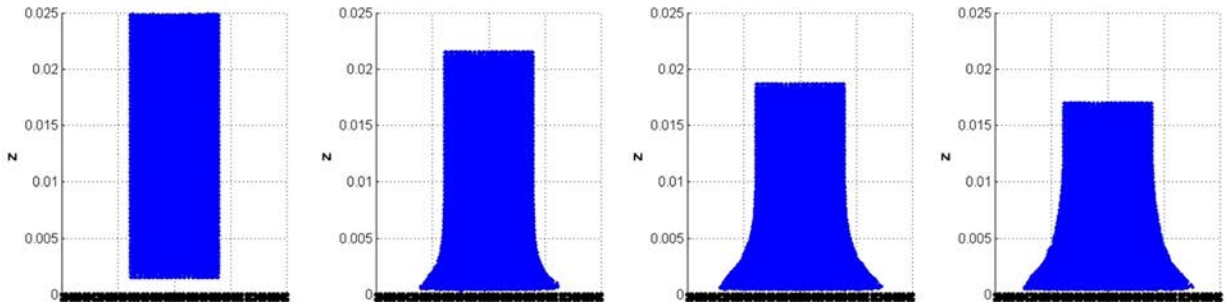

Fig. 17. Progress deformation of semi-Lagrangian RKPM computation.

Table 4. Comparison of deformed geometries for Taylor bar impact problem.

	Lagrangian RKPM*	Semi-Lagrangian RKPM	Experiment
Height (cm)	1.645	1.642	1.651
Radius (cm)	0.837	0.819	NA

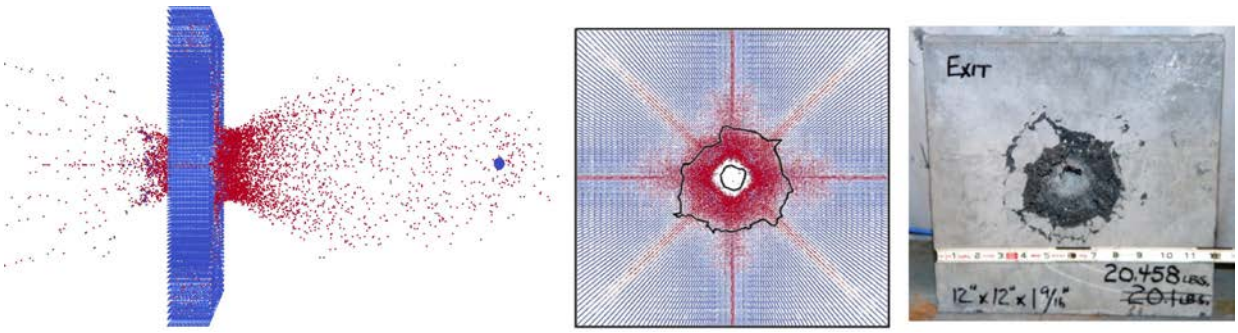

Fig. 18. Experimental and numerical damage patterns on the exit face of a concrete plate penetrated by a bullet.

Other attractive features in the presented RKPM meshfree methods include their flexibility in adaptive refinement [51] and in solving PDEs with higher order differentiation such as plates and shells [17, 47–49], contact problems due to the ability to describe contact surface with smooth functions [11], incompressible problems using node based projection method with optimal constraint ratio [6, 9, 10], localization problems with embedded gradient regularization in the meshfree approximation [12, 16], and shape optimization owing to the "meshfree" discretization [34, 35]. Radial basis functions in RBCM are also particularly effective in solving problems with high dimension [18].

5. Conclusion

Meshfree methods based on: 1) Galerkin type weak formulation with nodal integration such as RKPM and its stabilized counterparts and 2) strong formulation with collocation such as RBCM

and its variants have been presented. Approximation methods which do not require an underlined mesh connectivity structure, such as the reproducing kernel approximation, radial basis approximation, and localized radial basis approximation have been introduced to construct the finite dimensional spaces for meshfree methods, and their convergence properties have been discussed and compared in this work. Special attention has been devoted to the spatial instability resulting from rank deficiency of the nodally integrated Galerkin meshfree method as well as the ill-conditioning of strong form collocation method when global approximation functions such as the radial basis functions are used.

It is shown that with the proper treatment of the rank instability using stabilization methods such as SCNI and modified SCNI in the nodally integrated Galerkin meshfree method, the resulting numerical technique offers high accuracy and can be applied to problems where FEM is ineffective due to its regularity constraints. Fragment-impact problems presented in this paper are such examples. Meshfree methods based on strong form collocation, such as RBCM, are an attractive alternative due to their simplicity in implementation and the exponential convergence property. This class of meshfree methods, however, is suffering from its dense matrix and the associated ill-conditioning when performing model refinement. The nonlocality in the RBFs also weakens its applicability to problems with local features, for example, modelling of heterogeneous media and fractures. The recent advancements in the localized version of RBCM, namely, L-RBCM and RKCM, have shown to successfully remedy the above stated difficulties.

Mathematical analyses of meshfree methods for the above- mentioned challenging problems have not been well established and deserve special attention. Identification of problems where meshfree methods are particularly effective is also essential for the future advancement of this new class of computational methods.

Acknowledgement

The support of this work by U.S. Army Engineer Research and Development Center under the contract W912HZ-07-C-0019:P00001 to the first and second authors, and the support by National Science Council of Taiwan, R.O.C., under project number NSC 98-2115-M-029-001-MY2 to the third author are greatly acknowledged.

References

[1] S. Beissel, T. Belytschko. Nodal integration of the element-free Galerkin method. *Computer Methods in Applied Mechanics and Engineering*, **139**: 49–74, 1996.

[2] T. Belytschko, Y.Y. Lu, L. Gu. Element-free Galerkin methods. *International Journal for Numerical Methods in Engineering*, **37**: 229–256, 1994.

[3] T. Belytschko, Y. Krongauz, D. Organ, M. Fleming, P. Krysl. Meshless Methods: An Overview and Recent Development. *Comput. Meth. Appl. Mech. Engng.*, **139**: 3–49, 1996.

[4] J. Bonet, S. Kulasegaram. Correction and stabilization of smooth particle hydrodynamics methods with applications in metal forming simulation. *International Journal for Numerical Methods in Engineering*, **47**: 1189–1214, 1999.

[5] J.S. Chen, C. Pan, C.T. Wu, W.K. Liu. Reproducing Kernel Particle Methods for Large Deformation Analysis of Nonlinear Structures. *Computer Methods in Applied Mechanics and Engineering*, **139**: 195–227, 1996.

[6] J.S. Chen, C. Pan, C.T. Wu. Large Deformation Analysis of Rubber Based on a Reproducing Kernel Particle Method, *Computational Mechanics*, **19**: 211–227, 1997.

[7] J.S. Chen, C. Pan, C.M.O.L. Roque, H.P. Wang. A Lagrangian Reproducing Kernel Particle Method for Metal Forming Analysis. *Computational Mechanics*, **22**: 289-307, 1998.

[8] J.S. Chen, H.P. Wang. New boundary condition treatments for meshless computation of contact problems. *Computer Methods in Applied Mechanics and Engineering*, **187**: 441–468, 2000.

[9] J.S. Chen, H.P. Wang. Some Recent Improvements in Meshfree Methods for Incompressible Finite Elasticity Boundary Value Problems with Contact. *Computational Mechanics*, **25**: 137–156, 2000.

[10] J.S. Chen, S. Yoon, H.P. Wang, W.K. Liu. An Improved Reproducing Kernel Particle Method for Nearly Incompressible Hyperelastic Solids. *Computer Methods in Applied Mechanics and Engineering*, **181**: 117–145, 2000.

[11] J.S. Chen, H.P. Wang. New Boundary Condition Treatments for Meshless Computation of Contact Problems. *Computer Methods in Applied Mechanics and Engineering*, **187**: 441–468, 2000.
[12] J.S. Chen, C.T. Wu, T. Belytschko. Regularization of Material Instabilities by Meshfree Approximation with Intrinsic Length Scales. *International Journal for Numerical Methods in Engineering*, **47**: 1303–1322, 2000.
[13] J.S. Chen, C.T. Wu, S. Yoon, Y. You. A Stabilized Conforming Nodal Integration for Galerkin Meshfree Methods. *International Journal for Numerical Methods in Engineering*, **50**: 435–466, 2001.
[14] J.S. Chen, S. Yoon, C.T. Wu. Nonlinear Version of Stabilized Conforming Nodal Integration for Galerkin Meshfree Methods. *International Journal for Numerical Methods in Engineering*, **53**: 2587–2615, 2002.
[15] J.S. Chen, W. Han, Y.You, X. Meng. A reproducing kernel method with nodal interpolation property. *International Journal for Numerical Methods in Engineering*, **56**: 935–960, 2003.
[16] J.S. Chen, X. Zhang, T. Belytschko. An Implicit Gradient Model by a Reproducing Kernel Strain Regularization in Strain Localization Problems. *Computer Methods in Applied Mechanics and Engineering*, **193**: 2827–2844, 2004.
[17] J.S. Chen, D.D. Wang. A Constrained Reproducing Kernel Particle Formulation for Shear Deformable Shell in Cartesian Coordinate. *International Journal for Numerical Methods in Engineering*, **68**: 151–172, 2006.
[18] J.S. Chen, W. Hu, M. Puso. Orbital HP-Cloud for Schrödinger Equation in Quantum Mechanics. *Computer Methods in Applied Mechanics and Engineering*, **196**: 3693–3705, 2007.
[19] J.S. Chen, Y. Wu. Stability in Lagrangian and Semi-Lagrangian Reproducing Kernel Discretizations Using Nodal Integration in Nonlinear Solid Mechanics. In: V.M.A. Leitao, C.J.S. Alves, C.A. Duarte [Eds.], *Computational Methods in Applied Sciences*, 55–77. Springer, Oñate, Eugenio, 2007.
[20] J.S. Chen, W. Hu, H.Y. Hu. Reproducing Kernel Enhanced Local Radial Basis Collocation Method. *International Journal for Numerical Methods in Engineering*, **75**: 600–627, 2008.
[21] J.S. Chen, L. Wang, H.Y. Hu, S.W. Chi. Subdomain Radial Basis Collocation Method for Heterogeneous Media. *International Journal for Numerical Methods in Engineering*, **80**: 163–190, 2009.
[22] J.S. Chen, Y. Wu, P.C. Guan, H. Teng, J. Gaidos, K. Hofstetter, M. Alsaleh. A Semi-Lagrangian Reproducing Kernel Formulation for Modeling Earth Moving Operations. *Mechanics of Materials*, **41**: 670-683, 2009.
[23] J. Dolbow, T. Belytschko. Numerical integration of Galerkin weak form in meshfree methods. *Computational Mechanics*, **23**: 219–230, 1999.
[24] P.C. Guan, S.W. Chi, J.S. Chen, T.R. Slawson, M.J. Roth. Semi-Lagrangian Reproducing Kernel Particle Method for Fragment-Impact Problems, accepted. *International Journal of Impact Engineering*, 2011.
[25] W. Han, G.J. Wagner, W.K. Liu. Convergence analysis of a hierarchical enrichment of dirichlet boundary conditions in a meshfree method. *International Journal for Numerical Methods in Engineering*, **53**: 1323–1336, 2002.
[26] H.Y. Hu, Z.C. Li. Collocation methods for Poisson's equation. *Computer Methods in Applied Mechanics and Engineering*, **195**: 4139–4160, 2006.
[27] H.Y. Hu, J.S. Chen, W. Hu. Weighted Radial Basis Collocation Method for Boundary Value Problems. *International Journal for Numerical Methods in Engineering*, **69**: 2736–2757, 2007.
[28] H.Y. Hu., J.S. Chen, W. Hu. Error Analysis of Collocation Method Based on Reproducing Kernel Approximation. *Numerical Methods for Partial Differential Equations*, **27**: 554–580, 2011.
[29] H.Y. Hu, J.S. Chen. Perturbation and Stability Analysis of Strong Form Collocation with Reproducing Kernel Approximation. *International Journal for Numerical Methods in Engineering*, **88**: 157–179, 2011.
[30] A. Huerta, S. Fernandez-Mendez. Enrichment and coupling of the finite element and meshless methods. *International Journal for Numerical Methods in Engineering*, **48**: 1615–1636, 2000.
[31] I. Kaljevic, S. Saigal. An improved element free Galerkin formulation. *International Journal for Numerical Methods in Engineering*, **40**: 2953–2974, 1997.
[32] E.J. Kansa. Multiquadrics – A scattered data approximation scheme with applications to computational fluid-dynamics – I Surface approximations and partial derivatives. *Computers and Mathematics with Applications*, **19**: 127–145, 1992.
[33] E.J. Kansa. Multiquadrics – A scattered data approximation scheme with applications to computational fluid-dynamics – II Solutions to parabolic, hyperbolic and elliptic partial differential equations. *Computers and Mathematics with Applications*, **19**: 147–161, 1992.
[34] N.H. Kim, K.K. Choi, J.S. Chen. Shape Design Sensitivity Analysis and Optimization of Elasto-Plasticity with Frictional Contact. *AIAA*, **38**: 1742–1753, 2000.
[35] N.H. Kim, K.K. Choi, J.S. Chen. Die Shape Design of Sheet Metal Stamping Process Using Meshfree Method: Design Sensitivity Analysis. *International Journal for Numerical Methods in Engineering*, **51**: 1385–1405, 2001.
[36] Y. Krongauz, T. Belytschko. Enforcement of essential boundary conditions in meshless approximations using finite elements. *Computer Methods in Applied Mechanics and Engineering*, **131**: 133–145, 1996.
[37] W.K. Liu, S. Jun, Y.F. Zhang. Reproducing kernel particle methods. *International Journal for Numerical Methods in Fluids*, **20**: 1081–1106, 1995.
[38] W. R. Madych and S. A. Nelson. Bounds on multivariate polynomials and exponential error estimates for multiquadric interpolation. *Journal of Approximation Theory*, **70**: 94–114, 1992.

[39] J. Nitsche. Über ein Variationsprinzip zur Lösung von Dirichlet-Problemen bei Verwendung von Teilräumen, die keinen Randbedingungen unterworfen sind. Abh. Math. Sem. Univ. Hamburg, **36**: 9–15, 1971.
[40] M. Puso, E. Zywicz, J.S. Chen. A New Stabilized Nodal Integration Approach. *Lecture Notes in Computational Science and Engineering*, **57**: 207–218, 2006.
[41] M. Puso, J.S. Chen, E. Zywick, W. Elmer. Meshfree and Finite Element Nodal Integration Methods. *International Journal for Numerical Methods in Engineering*, **74**: 416–446, 2008.
[42] P.W. Randles, L.D. Libersky, A.G. Petschek. On neighbors, derivatives, and viscosity in particle codes. Proceeding of ECCM Conference, Munich, Germany, 31 August – 3 September, 1999.
[43] X. Ren, J.S. Chen, J. Li. Micro-cracks Informed Damage Models for Brittle Solids. accepted. *International Journal of Solids and Structures*, **48**: 1560–1571, 2011.
[44] M.J. Roth, J.S. Chen, T.R. Slawson, R.N. Boone, X. Ren, S.W. Chi, C.H. Lee, P.C. Guan. Multiscale RKPM Formulation for Modeling Penetration of an Ultra High-Strength Concrete Material. Proceeding, *Third International Conference on Computational Methods in Structural Dynamics and Earthquake Engineering*, May 26–28, 2011, Corfu, Greece.
[45] R. Schaback, H. Wendland. Using compactly supported radial basis functions to solve partial differential equations. *Boundary Element Technology XIII*, 1999.
[46] S.P. Timoshenko, J.N. Goodier, *Theory of Elasticity*. McGraw-Hill. New York, USA, 1970.
[47] D. Wang, J.S. Chen. Locking Free Stabilized Conforming Nodal Integration for Meshfree Mindlin-Reissner Plate Formulation. *Computer Methods in Applied Mechanics and Engineering*, **193**: 1065–1083, 2004.
[48] D. Wang, J.S. Chen. A Locking-free Meshfree Curved Beam Formulation with the Stabilized Conforming Nodal Integration. *Computational Mechanics*, **39**: 83–90, 2006.
[49] D. Wang, J.S. Chen. A Hermite Reproducing Kernel Approximation for Thin Plate Analysis with Sub-domain Stabilized Conforming Integration. *International Journal for Numerical Methods in Engineering*, **74**: 368–390, 2008.
[50] L. Wang, J.S. Chen, H.Y. Hu. Subdomain Radial Basis Collocation Method for Fracture Mechanics. *Int. J. Numer. Meth. Engng.*, **83**: 851–876, 2010.
[51] Y. You, J.S. Chen, H. Lu. Filter, Reproducing Kernel, and Adaptive Meshfree Methods. *Computational Mechanics*, **31**: 316-326, 2003.
[52] T. Zhu, S.N. Atluri. A modified collocation method and a penalty formulation for enforcing the essential boundary conditions in the element free Galerkin method. *Computational Mechanics*, **21**: 211–222, 1998.
[53] W. Han, X. Meng. Error analysis of the reproducing kernel particle method. *Computer Methods in Applied Mechanics and Engineering*, **190**: 6157-–6181, 2001.